

CONVEX PROGRAMMING APPROACH OF ROBUST POWERED DESCENT GUIDANCE THROUGH DYNAMIC TUBE MPC

Jaell Jang¹, Chang-Hun Lee¹ & Shaoming He²

¹Korea Advanced Institute of Science and Technology (KAIST), Daejeon 34141, Republic of Korea ²Beijing Institute of Technology, Beijing 100081, P.R. China

Abstract

This paper presents robust powered descent guidance(PDG) algorithm based on dynamic tube model predictive control(MPC). Employing the dynamic tube MPC as a baseline guidance methodology, the modeling error and disturbances are explicitly considered in the MPC problem and the robust control invariant tube geometry is simultaneously optimized along with the original powered descent guidance states. Furthermore, the proposed robust PDG problem is transformed into convex optimization framework through sequential convex programming(SCP) algorithm which is suitable form for real-time application. In the end, numerical experiments are carried out to validate the performance and robustness of the proposed PDG algorithm.

Keywords: Robust powered descent guidance, Dynamic tube MPC, Sequential convex programming

1. Introduction

Powered descent guidance(PDG) is a key technology to achieve precise soft landing of reusable launch vehicle(RLV). For effective and successful PDG implementation, guidance command should satisfy optimality in fuel consumption for landing with limited fuel and adhere to several path constraints to ensure vehicle safety during the flight[1]. To meet these requirements, applying convex optimization based computational guidance and control schemes[2] to the PDG algorithm has being actively researched[3, 4, 5, 6]. Since convex optimization problem can guarantee global optimality and leverages algorithm with polynomial time convergence, such as interior-point method[7], it is well-suited for PDG algorithm that requires real-time onboard computation of the optimal guidance commands. However, the fidelity of the model significantly influences the performance and robustness of the algorithm because computational guidance schemes derive solutions based on system model information[2]. Unfortunately, uncertainties from model errors and disturbances, such as aerodynamic coefficient errors and wind, arise during the landing process and the trade-off between the problem's complexity and model fidelity may restrict the use of high-fidelity models. These factors can degrade the performance of the guidance algorithm and, in severe cases, lead to its failure.

To derive a robust guidance algorithm that can efficiently handle disturbances and uncertainties, this paper introduces a robust PDG algorithm based on the dynamic tube MPC[8]. Dynamic tube MPC incorporates the boundary layer sliding mode controller as an ancillary controller, enhancing robustness against disturbances and uncertainties. As sliding mode control is a nonlinear controller, it can directly handle the nonlinear dynamics without linearization. Moreover, robust control invariant(RCI) tube and control bandwidth are simultaneously optimized based on the currents states and uncertainty level in the dynamic tube MPC. This allows to handle disturbances and uncertainties with reduced conservativeness. For a practical implementation of the proposed PDG algorithm, a model predictive guidance structure that divides the process into trajectory planning and tracking phase[9] is adopted in this paper. The reference trajectory and control inputs are initially determined through the trajectory planning phase. Subsequently, a model predictive control(MPC) scheme generates

the control commands, aiming to adhere to the reference trajectory based on a feedback of the current state, which may deviate from the planned path. The proposed algorithm utilizes dynamic tube MPC for trajectory tracking phase, instead of nominal MPC, so that it can explicitly consider external disturbances and model uncertainties. Therefore, it can ensure a safe, precise landing and robust trajectory tracking performance in the presence of disturbances and model errors. Then, the proposed robust PDG problem is transformed into convex optimization framework by using the lossless convexification[3] and sequential convex programming[10], allowing the problem to be suitable for real-time implementation.

The remainder of the paper is organized as follow. Section 2 introduces the dynamics model and constraints for the powered descent guidance problem. Section 3 presents the robust powered descent guidance problem based on the dynamic tube MPC scheme and convex formulation of the robust PDG problem is described in section 4. In section 5, the results of numerical experiments to verify the performance and robustness of proposed algorithm are depicted. Lastly, the conclusion of this paper is provided in section 6.

2. Powered Descent Guidance Problem

Before getting into the description of the PDG problem for trajectory tracking, we introduce the assumptions made for the problem formulation in this paper.

- Assumption 1. Non-rotating flat Earth with uniform gravitational field is assumed since the powered descent guidance phase begins at relatively low altitude and takes short times.
- Assumption 2. The thrust is assumed to be aligned with the longitudinal axis of the body since the thrust deflection angle is small and the roll attitude is well regulated in 0°.
- Assumption 3. The dynamics can be expressed in control affine form $\dot{x} = f(x) + b(x)u + d$, where $x \in \mathbb{R}^n$ is the states, $u \in \mathbb{R}^n$ is the control input and $d \in \mathbb{R}^n$ is the external disturbances.
- Assumption 4. The dynamics f(x) can be expressed by $f(x) = \hat{f}(x) + \tilde{f}(x)$ where \hat{f} is the nominal dynamics incorporating the best estimates of model parameters and $\tilde{f}(x)$ is the bounded model uncertainties where $|\tilde{f}(x)| \leq \Delta(x)$.
- Assumption 5. The external disturbances d belong to the closed, bounded and connected set $\mathbb{D} = \{d \in \mathbb{R}^n : |d| \leq D\}$ and $d \in \text{span}(b(x))$.
- Assumption 6. The reference trajectory for powered descent guidance is well established through the explicit trajectory planning problem and this paper only focuses on developing methodology for the trajectory tracking problem.

2.1 Dynamics Model

The 3-DOF translational dynamics model is used to describe the motion of RLV. The equations of motion are expressed in the inertial NED(North-East-Down) frame with the origin at the desired landing position as in Figure 1.

From the assumptions, the translational dynamics in the presence of external disturbances and model uncertainties can be written as,

$$\ddot{r}(t) = \left[\frac{1}{m(t)} \left(-\frac{1}{2} \rho \left(\hat{C}_d + \tilde{C}_d \right) S_{ref} \| \dot{r}(t) \|_2 \dot{r}(t) \right) + g \right] + \frac{1}{m(t)} T(t) + d$$
(1)

$$\dot{m}(t) = -\frac{\|T(t)\|_2 + P_{atm}A_e}{I_{sp}g_0} \tag{2}$$

where $r(t) \in \mathbb{R}^3$ is the position vector, $\dot{r}(t) \in \mathbb{R}^3$ is the velocity vector of the vehicle with respect to the reference frame, $m(t) \in \mathbb{R}$ is the mass of the vehicle, $T(t) \in \mathbb{R}^3$ is the thrust vector considering the reduction of thrust by atmospheric pressure, $g \in \mathbb{R}^3$ is the constant gravitational acceleration, ρ is the air density, S_{ref} is the reference area for an aerodynamic drag force, P_{atm} is the atmospheric

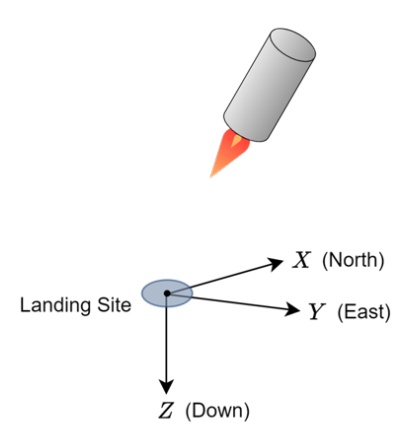


Figure 1 – Reference frame (Inertial NED frame)

pressure, A_e is the exit area of the rocket engine, I_{sp} is the specific impulse of the engine and g_0 is the standard gravity at the Earth's surface. \hat{C}_d is a nominal value of drag coefficient and \tilde{C}_d is a bounded uncertainty in drag coefficient. $d \in \mathbb{R}^3$ is a bounded external disturbances, representing the effects of wind or unmodeled dynamics such as lift. For conciseness and clarity, let the states vector and control vector be defined as

$$x(t) = \begin{bmatrix} r(t) & \dot{r}(t) & m(t) \end{bmatrix}^T, \qquad u(t) = T(t)$$
(3)

Then, equation (1) can be expressed as

$$\ddot{r}(t) = f(x(t)) + b(x(t))u(t) + d \tag{4}$$

where b(x(t)) = diag(1/m(t), 1/m(t), 1/m(t)) and the dynamics $f = \hat{f} + \tilde{f}$ is consisted of the nominal dynamics \hat{f} and bounded uncertain dynamics \tilde{f} as follow.

$$\hat{f}(x(t)) = \frac{1}{m(t)} \left(-\frac{1}{2} \rho \hat{C}_d S_{ref} || \dot{r}(t) ||_2 \dot{r}(t) \right) + g$$
 (5)

$$\tilde{f}(x(t)) = \frac{1}{m(t)} \left(-\frac{1}{2} \rho \tilde{C}_d S_{ref} || \dot{r}(t) ||_2 \dot{r}(t) \right) \le \Delta(x(t))$$
(6)

2.2 Constraints and Cost Function

In this subsection, the constraints to obtain physically feasible solution and to ensure safe landing are introduced. First, the thrust magnitude is bounded as

$$0 < T_{min} - P_{atm} A_e \le ||T(t)||_2 \le T_{max} - P_{atm} A_e \tag{7}$$

Since the typical solution form of the propellant-optimal powered descent guidance is the bang-bang control profile[3], which may be physically restricted by the engine properties, the rate of thrust magnitude change constraint is imposed as follow.

$$-\dot{T}_{\max} \le \frac{d\|T(t)\|_2}{dt} \le \dot{T}_{\max} \tag{8}$$

To ensure the stability during the powered descent, tilt angle constraints based on Assumption 2 is considered.

$$-T_z(t) \ge ||T(t)||_2 \cos \theta_{\text{max}} \tag{9}$$

where T_z is the z-component of the thrust represented in inertial NED frame and θ_{max} is a maximum tilt angle. Similarly, the angle of attack(AoA) constraint is imposed to prevent excessive aerodynamic loads, with a maximum allowable AoA denoted as α_{max} .

$$-T(t)^{T}\dot{r}(t) + ||T(t)||_{2}||\dot{r}(t)||_{2}\cos\alpha_{\max} \le 0$$
(10)

The cost function to track the reference trajectory is formulated as a quadratic form of tracking error.

$$J = \int_{t_0}^{t_f} \left[r(t) - r^*(t) \right]^T Q \left[r(t) - r^*(t) \right] + \left[u(t) - u^*(t) \right]^T R \left[u(t) - u^*(t) \right] dt \tag{11}$$

where $r^*(t)$ and $u^*(t)$ is the reference position and control input, which are determined from a separated trajectory planning phase.

2.3 Powered Descent Guidance Problem for Trajectory Tracking Phase

Based on the dynamics and constraints, the optimal control problem for powered descent guidance during the trajectory tracking phase can be formulated as follow.

Problem 1: Powered Descent Guidance for Trajectory Tracking

minimize
$$J = \int_{t_0}^{t_f} \left[r(t) - r^*(t) \right]^T Q \left[r(t) - r^*(t) \right] + \left[u(t) - u^*(t) \right]^T R \left[u(t) - u^*(t) \right] dt$$
 subject to
$$\ddot{r}(t) = \hat{f} \left(x(t) \right) + \tilde{f} \left(x(t) \right) + b \left(x(t) \right) u(t) + d$$

$$\dot{m}(t) = -\frac{\|T(t)\|_2 + P_{atm} A_e}{I_{sp} g_0}$$

$$r(t_0) = r_0, \ \dot{r}(t_0) = \dot{r}_0, \ m(t_0) = m_0$$

$$T_{\min} - P_{atm} A_e \leq \|T(t)\|_2 \leq T_{\max} - P_{atm} A_e$$

$$- \dot{T}_{\max} \leq \frac{d \|T(t)\|_2}{dt} \leq \dot{T}_{\max}$$

$$T_z(t) + \|T(t)\|_2 \cos \theta_{\max} \leq 0$$

$$- T(t)^T \dot{r}(t) + \|T(t)\|_2 \|\dot{r}(t)\|_2 \cos \alpha_{\max} \leq 0$$

3. Dynamic Tube MPC for Robust Powered Descent Guidance

3.1 Ancillary Controller

This subsection overviews the boundary layer sliding mode controller which is used as an ancillary controller in dynamic tube MPC[8]. Let $\tilde{r}(t) := r(t) - r^*(t)$ be the tracking error for the position. Then, the sliding variable s_i for the states r_i can be defined as

$$s_i(t) = \left(\frac{d}{dt} + \lambda_i\right)\tilde{r}_i(t) = \dot{\tilde{r}}_i(t) + \lambda_i\tilde{r}_i(t) = \dot{r}_i(t) - \dot{r}_{r,i}(t) \qquad \text{for } i = \{1, 2, 3\}$$
 (12)

where $\lambda_i > 0$ is the positive slope of the sliding surface and $\dot{r}_r(t) = \dot{r}_i^*(t) - \lambda_i \tilde{r}_i(t)$. For $s_i(t)$, the sliding surface is defined such that $s_i(t) = 0$ which makes the tracking error exponentially converge to 0 as it reaches the sliding surface. However, high frequency chattering problem in the control input may arise due to the modeling imprecision and disturbances in the sliding mode controller[11]. To avoid chattering problem, a time-varying boundary layer is introduced around the sliding surface. The boundary layer with thickness $\Phi_i(t)$ can be defined as

$$\mathbb{B}_i := \{ r(t) : |s_i(t)| \le \Phi_i(t) \} \tag{13}$$

and the boundary layer is attractive if the following condition holds.

$$\frac{1}{2}\frac{d}{dt}s_i^2 \le \left(\dot{\Phi}_i - \eta_i\right)|s_i| \tag{14}$$

where η_i is the convergence rate to the sliding surface. Then, the dynamics of the sliding variable can be obtained by differentiating (12) as

$$\dot{s}_i = \ddot{r}_i - \ddot{r}_{r,i} = f_i(x) + \sum_{j=1}^3 b_{ij}(x)u_j + d_i - \ddot{r}_{r,i}$$
(15)

By expressing equation (15) into a vector form,

$$\dot{s} = f(x) + b(x)u + d - \ddot{r}_r \tag{16}$$

Note that $b(x) \in \mathbb{R}^{3\times 3}$ is a diagonal matrix and thus invertible. The control law for the boundary layer sliding mode controller is given as a form of

$$u = b^{-1}(x) \left[-\hat{f}(x) + \ddot{r}_r - K(x) \circ sat \left(s \oslash \Phi \right) \right]$$
(17)

where \circ and \oslash operator is the Hadamard product and division. From (14), the boundary layer is attractive for $|s| > \Phi$ if

$$K(x) = \Delta(x) + D + \eta - \dot{\Phi} \tag{18}$$

For the sliding variable within the boundary layer $|s| \le \Phi$, the sliding variable dynamics can be expressed as follow.

$$\dot{s} = -(K(x) \oslash \Phi) \circ s + f(x) - \hat{f}(x) + d \tag{19}$$

or

$$\dot{s} = -(K(x^*) \oslash \Phi) \circ s + (f(x^*) - \hat{f}(x^*) + d + O(\tilde{x})) \tag{20}$$

which is a first order filter with cut-off frequency $K(x^*) \oslash \Phi$. For the desired cut-off frequency κ , the boundary layer dynamics can be obtained as

$$\dot{\Phi} = -\kappa \circ \Phi + \Delta(x^*) + D + \eta \tag{21}$$

From the **Theorem 1** in [8], the robust control invariant(RCI) tube Ω_i is induced as

$$\Omega_i(t) \le e^{-\lambda_i(t-t_0)}\Omega_i(t) + \int_{t_0}^t e^{-\lambda_i(t-t_0-\tau)}\Phi_i d\tau \tag{22}$$

We can notice, from (19) and (21), that higher κ produces tighter boundary layer thickness but increases the effect of the uncertainties and disturbances. Consequently, κ is designated as a decision variable in the optimization process allowing for the appropriate value of κ to be chosen based on the current states. To obtain continuous and smooth control input, κ is assumed to follow auxiliary dynamics relation[8]

$$\dot{\kappa}(t) = w \tag{23}$$

where w is the slack variable which is determined from the optimization process.

3.2 Constraints Tightening

States and control constraints should be tightened in dynamic tube MPC problem to prevent the constraints violation by the ancillary controller due to disturbances[8]. From (17), the control input can be rewritten as

$$u = u^* + u_{fb} = u^* + b^{-1} \left[\hat{f}(x^*) - \hat{f}(x) - \lambda \circ \hat{r} - K(x) \circ sat(s \oslash \Phi) \right]$$
 (24)

where u^* is the feedforward control input from the MPC solution and u_{fb} is the feedback control by the ancillary controller. The upper bound of u_{fb} can be obtained as

$$u_{fb} \le b^{-1} \left[\frac{1}{2m} \rho \hat{C}_d S_{ref} \left(\|\dot{r}^*\|_2 \dot{\tilde{r}}_{max} + \|\dot{\tilde{r}}_{max}\|_2 \dot{r}^* \right) - \lambda \circ \dot{\tilde{r}} - \kappa \circ \Phi \right] := \tilde{u}_{max}$$
 (25)

From the definition of the sliding variable s, the upper bound of magnitude of velocity tracking error is calculated as

$$|\dot{\tilde{r}}_i| = |s_i - \lambda_i \tilde{r}_i| \le \Phi_i + \lambda_i \Omega_i \tag{26}$$

Using (26), $|\tilde{u}_{max}|$ can be expressed

$$|\tilde{u}_{max,i}| = b^{-1} \left[\frac{1}{2m} \rho \hat{C}_d S_{ref} (\|\dot{r}^*\|_2 (\Phi_i + \lambda_i \Omega_i) + \|\Phi_i + \lambda_i \Omega_i\|_2 \dot{r}^*) - \lambda_i \Phi_i - \lambda_i^2 \Omega_i - \kappa_i \Phi_i \right]$$
(27)

Then, the control constraints can be tightened as

$$T_{min} - P_{atm}A_e + \|\tilde{u}_{max}(t)\|_2 \le \|T(t)\|_2 \le T_{max} - P_{atm}A_e - \|\tilde{u}_{max}(t)\|_2$$
(28)

3.3 Robust Powered Descent Guidance Problem

The robust powered descent guidance problem based on the dynamic tube MPC can be formulated as **Problem 2**. The tightened control constraint is applied and the tube geometry is simultaneously optimized along with the original state in PDG problem leveraging the state-dependent uncertainties[8]. The cost function is augemented by adding the penalizing term for the controller bandwidth and the constraints for the control bandwidth are newly added.

Problem 2: Robust Powered Descent Guidance for Trajectory Tracking

$$\begin{split} & \underset{u(t),w(t)}{\text{minimize}} & J = \int_{t_0}^{t_f} \left[r(t) - r^*(t) \right]^T Q \left[r(t) - r^*(t) \right] + \left[u(t) - u^*(t) \right]^T R \left[u(t) - u^*(t) \right] \\ & + \left[\kappa(t) - \kappa_{min} \right]^T M \left[\kappa(t) - \kappa_{min} \right] dt \end{split} \\ & \text{subject to} \\ & \ddot{r}(t) = \hat{f} \left(x(t) \right) + b \left(x(t) \right) u(t) \\ & \dot{m}(t) = -\frac{\| T(t) \|_2 + P_{atm} A_e}{I_{sp} g_0} \\ & \dot{\Phi}(t) = -\kappa(t) \circ \Phi(t) + \Delta(x(t)) + D + \eta \\ & \dot{\Omega}(t) = -\lambda \circ \Omega(t) + \Phi(t), \ \dot{\kappa}(t) = w(t) \\ & r(t_0) = r_0, \ \dot{r}(t_0) = \dot{r}_0, \ m(t_0) = m_0 \\ & \Phi(t_0) = \Phi_0, \ \Omega(t_0) = |\tilde{r}(t_0)|, \ \kappa(t_0) = \kappa_0 \\ & T_{min} - P_{atm} A_e + \| \tilde{u}_{max} \|_2 \leq \| T(t) \| \leq T_{max} - P_{atm} A_e - \| \tilde{u}_{max} \|_2 \\ & - \dot{T}_{max} \leq \frac{d \| T(t) \|_2}{dt} \leq \dot{T}_{max}, \quad T_z(t) + \| T(t) \|_2 \cos \theta_{max} \leq 0 \\ & - T(t)^T \dot{r}(t) + \| T(t) \|_2 \| \dot{r}(t) \|_2 \cos \alpha_{max} \leq 0 \\ & \kappa_{min} \leq \kappa(t) \leq \kappa_{max}, \quad - \dot{\kappa}_{max} \leq w(t) \leq \dot{\kappa}_{max} \end{split}$$

4. Convex Formulation of Robust Powered Descent Guidance Problem

Since the **Problem 2** should be repeatedly solved for the MPC approach, formulating the problem into convex optimization framework is desirable. However, the proposed robust powered descent guidance problem (**Problem 2**) is non-convex due to nonlinear dynamics and non-convex inequality constraints. Thus, convexification technique such as lossless convexification[3] and sequential convex programming[10] is applied to obtain the convexified problem.

4.1 Lossless Convexification of Thrust Magnitude Constraints

The thrust magnitude constraints (7) is non-convex due to its lower bound and this non-convexity can be handled without linearization through lossless convexification technique[3]. By introducing the slack variable $\Gamma \in \mathbb{R}$, the non-convex thrust magnitude constraints can be relaxed as

$$||T(t)||_2 \le \Gamma(t) \tag{29}$$

$$T_{min} - P_{atm}A_e \le \Gamma(t) \le T_{max} - P_{atm}A_e \tag{30}$$

Then, the tightened control constraints(28) can be replaced as

$$T_{min} - P_{atm}A_e + \|\tilde{u}_{max}(t)\|_2 \le \Gamma(t) \le T_{max} - P_{atm}A_e - \|\tilde{u}_{max}(t)\|_2$$
(31)

or

$$\|\tilde{u}_{max}(t)\|_{2} \le \Gamma(t) - (T_{min} - P_{atm}A_{e}) \tag{32}$$

$$\|\tilde{u}_{max}(t)\|_2 \le -\Gamma(t) + (T_{max} - P_{atm}A_e) \tag{33}$$

Note that \tilde{u}_{max} is still non-convex and if \tilde{u}_{max} is linearized, equation (32) and (33) become standard form of second-order cone constraints. Moreover, thrust magnitude in other constraints can be replaced into Γ .

4.2 Linearization and Discretization

Let $X = \begin{bmatrix} r \ , \dot{r} \ , m \ , \Phi \ , \Omega \ , \kappa \end{bmatrix}^T$ be the state and $U = \begin{bmatrix} T \ , \Gamma \ , w \end{bmatrix}^T$ be the control vector of the **Problem 2**. Then, the dynamics of **Problem 2** including the tube dynamics can be expressed in vector form as

$$\dot{X} = F(X, U) \tag{34}$$

$$F(X,U) := \begin{bmatrix} \dot{r}(t) \\ \hat{f}(x(t)) + b(x(t)) u(t) \\ -\frac{\Gamma(t) + P_{atm} A_e}{I_{sp} g_0} \\ -\kappa(t) \circ \Phi(t) + \Delta(x(t)) + D + \eta \\ -\lambda \circ \Omega(t) + \Phi(t) \\ w(t) \end{bmatrix}$$
(35)

With reference state and control \bar{X} , \bar{U} , the dynamics can be linearized as

$$\dot{X} = AX + BU + D \tag{36}$$

where

$$A := \frac{\partial F}{\partial X}\Big|_{(\bar{X},\bar{U})}, \quad B := \frac{\partial F}{\partial U}\Big|_{(\bar{X},\bar{U})}, \quad D := F(\bar{X},\bar{U}) - A\bar{X} - B\bar{U}$$
(37)

Then, the linearized dynamics can be discretized by using trapezoidal rule with discrete time node $k \in \{0, 1, ..., N\}$.

$$X_{k+1} = X_k + \frac{\Delta t}{2} \left(\left[A_k X_k + B_k U_k + D_k \right] + \left[A_{k+1} X_{k+1} + B_{k+1} U_{k+1} + D_{k+1} \right] \right) \tag{38}$$

For constraints, only non-convex components are linearized with reference state and control. Let h_i denote the non-convex component in the constraints such as \tilde{u}_{max} . Then, it can be linearized with \bar{X} and \bar{U} as

$$h_i(X,U) \simeq A_{h_i}X + B_{h_i}U + D_{h_i} \tag{39}$$

where

$$A_{h_i} := \left. \frac{\partial h_i}{\partial X} \right|_{(\bar{X},\bar{U})}, \ B_{h_i} := \left. \frac{\partial h_i}{\partial U} \right|_{(\bar{X},\bar{U})}, \ D_{h_i} := h_i(\bar{X},\bar{U}) - A_{h_i}\bar{X} - B_{h_i}\bar{U}$$

$$\tag{40}$$

and the convexified constraints are imposed on every discrete time node k.

4.3 Convex Subproblem

The sequential convex programming derives the solution by sequentially solving the convex subproblem which can be constructed by linearizing the non-convex components in the original problem. The subproblem solution of current iteration is used as a reference point of linearization in the next subproblem, and this successive process is repeated until the solution converges. The convex subproblem for robust powered descent guidance problem is formulated in **Problem 3**. The soft quadratic trust region is added to maintain the validity of linearization and to avoid the artificial unboundedness problem that may arise from the linearization process.

$$J_{tr} = \sum_{k=1}^{N} \left([X_k - \bar{X}_k]^T W_X [X_k - \bar{X}_k] + [U_k - \bar{U}_k]^T W_U [U_k - \bar{U}_k] \right)$$
(41)

where W_X and W_U is the positive definite weighting matrix for the trust region radius. The resulting convex subproblem(**Problem 3**) is formulated in second-order cone programming(SOCP) and it can be efficiently handled by the interior-point algorithm.

Problem 3: Convex Subproblem of Robust Powered Descent Guidance Problem

$$\begin{aligned} & \text{minimize} & & J = \sum_{k=0}^{N} \left([X_k - X_k^*]^T Q'[X_k - X_k^*] + [U_k - U_k^*]^T R'[U_k - U_k^*] \right) + J_{tr} \\ & \text{subject to} & & X_{k+1} = X_k + \frac{\Delta t}{2} \left([A_k X_k + B_k U_k + D_k] + [A_{k+1} X_{k+1} + B_{k+1} U_{k+1} + D_{k+1}] \right) & \forall k \in \{0, 1, ..., N-1\} \\ & & X_0 = \begin{bmatrix} r_0, \ \dot{r}_0, \ m_0, \ \Phi_0, \ \Omega_0, \ \kappa_0 \end{bmatrix}^T \\ & & \|A_{\tilde{u}_{max}, k} X_k + B_{\tilde{u}_{max}, k} U_k + D_{\tilde{u}_{max}, k} \|_2 \leq \Gamma_k - (T_{min} - P_{atm} A_e) & \forall k \in \{0, 1, ..., N\} \\ & & \|A_{\tilde{u}_{max}, k} X_k + B_{\tilde{u}_{max}, k} U_k + D_{\tilde{u}_{max}, k} \|_2 \leq -\Gamma_k + (T_{max} - P_{atm} A_e) & \forall k \in \{0, 1, ..., N\} \\ & & \|T_k\|_2 \leq \Gamma_k, \ -\dot{T}_{max} \Delta t \leq \Gamma_{k+1} - \Gamma_k \leq \dot{T}_{max} \Delta t & \forall k \in \{0, 1, ..., N-1\} \\ & & T_{z,k} + \Gamma_k \cos\theta_{max} \leq 0, \ A_{aoa,k} X_k + B_{aoa,k} U_k + D_{aoa,k} \leq 0 & \forall k \in \{0, 1, ..., N\} \\ & \kappa_{min} \leq \kappa_k \leq \kappa_{max}, \ -\dot{\kappa}_{max} \leq w_k \leq \dot{\kappa}_{max} & \forall k \in \{0, 1, ..., N\} \end{aligned}$$

5. Numerical Experiments

The numerical experiments are carried out to validate the performance and robustness of the proposed PDG algorithm. The convex subproblem described in **Problem 3** is solved by using the ECOS[12] in MATLAB and the SCP algorithm is initialized with naive straight-line initial guess. Table 1 presents the parameters used in the numerical experiments.

| Parameter | Values | Parameter | Values |
|--------------------------------|----------------------------------|--|-------------------------------------|
| Initial Position (r_0) | [48, 48, -1200] ^T (m) | Sliding Surface Slope (λ) | $[1.2, 1.2, 1.2]^T (s^{-1})$ |
| Initial Velocity (\dot{r}_0) | $[-13.2, -13.2, 200]^T$ (m/s) | Sliding Surface Convergence Rate (η) | $[1.2, 1.2, 1.2]^T (s^{-2})$ |
| Initial Mass (m_0) | 14,000 (kg) | Disturbance Bound (D) | [1.0, 1.0, 1.0] (m/s ²) |
| Max. Thrust (T_{max}) | 360 (kN) | C_d uncertainties (\tilde{C}_d) | 10 (%) |
| Min. Thrust (T_{min}) | 144 (kN) | Control Bandwidth Lower Bound (κ_{min}) | $0.5 (s^{-1})$ |
| Max. Thrust Rate (T_{max}) | 198.5 (kN/s) | Control Bandwidth Upper Bound (κ_{max}) | 10 (s^{-1}) |
| | | Max. Control Bandwidth Rate $(\dot{\kappa}_{max})$ | $0.5 (s^{-2})$ |

Table 1 – Simulation parameters

| Dispersion Sources | Description | |
|------------------------------------|---|--|
| (A) Initial States Deviation | Deviations in initial position in the range of [-15, 15] (m), initial velocity in the range of [-3, 3](m/s) and initial mass in the range of [-2.5, 2.5](%) | |
| (B) Aerodynamics Coefficient Error | Uniformly distributed aerodynamics coefficient error in the range of [-10, 10](%) | |
| (C) Wind | Uniformly distributed wind speed in the range of [0, 5] (m/s) which affects the angle of attack and dynamic pressure | |
| (D) External Disturbance | External disturbances in uniformly distributed bounded disturbance set $\mathbb D$ in the range of [-1, 1](m/s^2) | |

Table 2 - Dispersion Sources

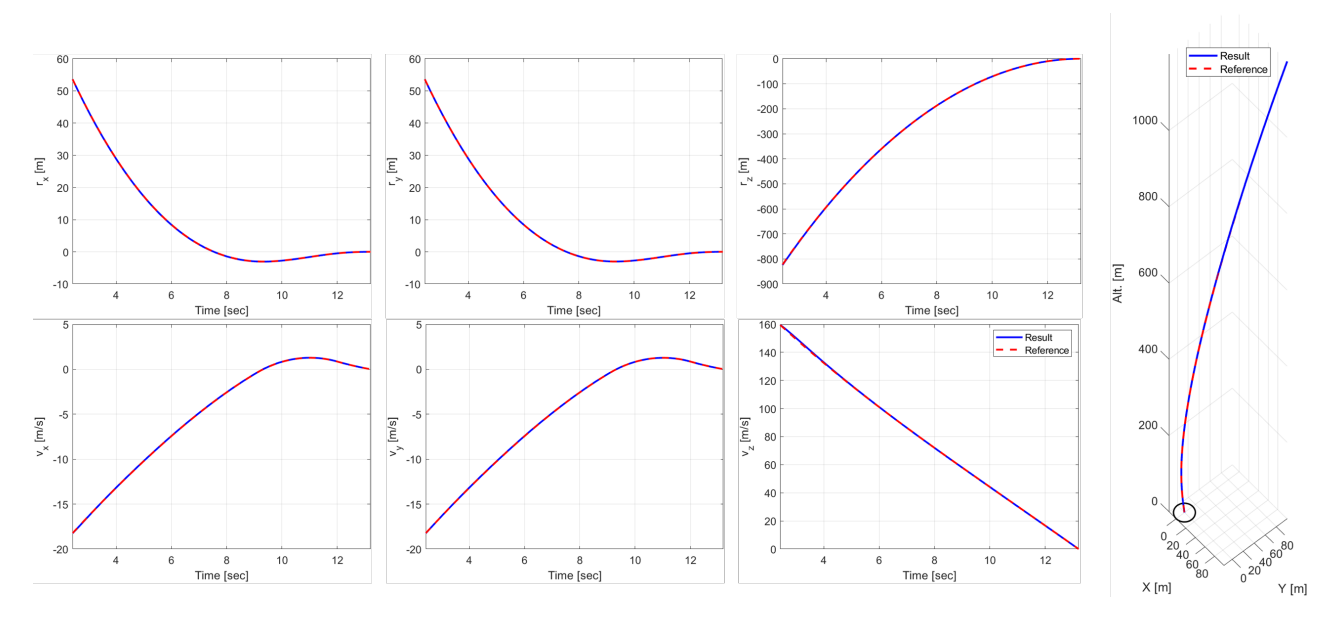


Figure 2 – States and trajectory (Baseline Case)

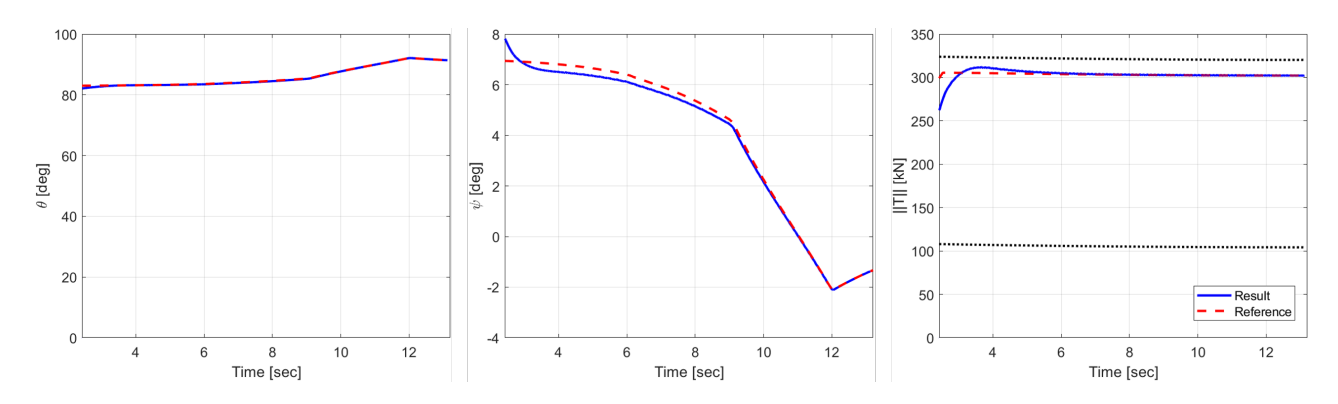


Figure 3 – Thrust magnitude and attitude (Baseline Case)

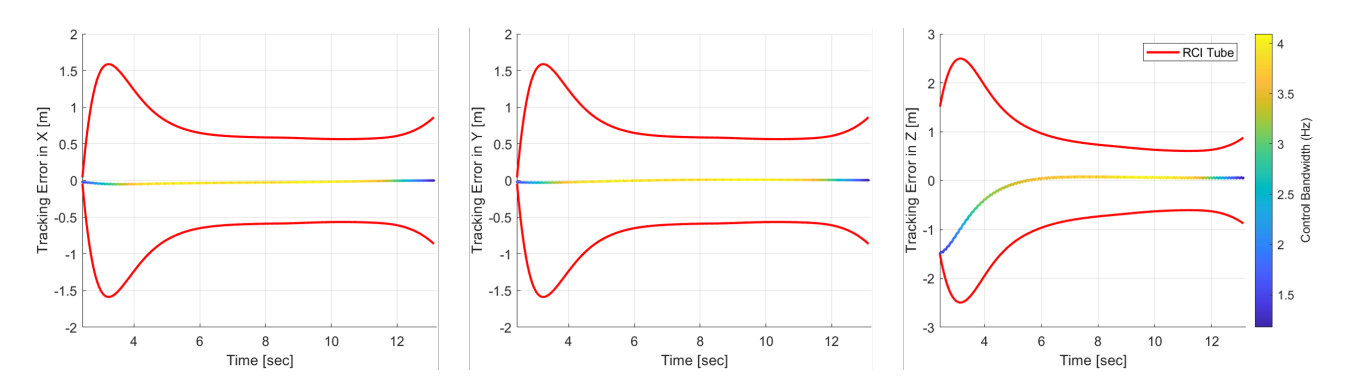


Figure 4 – Position tracking error and RCI tube (Baseline Case)

5.1 Baseline Case

The numerical experiments are carried out for a baseline case to validate the nominal performance of the proposed guidance. In the baseline scenario, the simulation is performed using the nominal dynamics model, incorporating additional aerodynamic forces such as lift and side force to assess the effects of unmodeled dynamics in the MPC model.

Figure 2 presents the states and trajectory of RLV during the powered descent phase, and Figure 3 depicts the thrust control input from the proposed robust powered descent guidance. The red dashed line represents the reference states established by the explicit trajectory planning problem following

the Assumption 6. The attitude angle in Figure 3 is calculated as

$$\psi = \sin^{-1}\left(\frac{T_y}{\|T\|}\right), \ \theta = \tan^{-1}\left(\frac{-T_z}{T_x}\right)$$
 (42)

based on Assumption 2.

Figure 4 presents the tracking error results and RCI tube from the robust powered descent guidance algorithm. The optimal control bandwidth κ^* is described as a color map where high bandwidth is mapped into yellow and low bandwidth is into blue. It can be observed that the tracking error converges to 0 and remains bounded within the RCI tube despite the initial error with the reference trajectory and unmodeled dynamics due to additional aerodynamic forces. It is also worth noting that the tube size is adjusted based on the magnitude of the tracking error, and accordingly, the control bandwidth κ is modified to bound the tracking error within the RCI tube.

5.2 Maximum Disturbance Case

In this case, the simulation was conducted under conditions with a disturbance of [1.0, 1.0, 1.0] m/s² and a 10% error in aerodynamic coefficients, which are the maximum values considered during the PDG design. As shown in Figure 5, the tracking error initially increases due to external disturbances and modeling error. However, it is eventually bounded within the tube by dynamic tube MPC. Additionally, as the tube tightens, the control bandwidth κ is increased to ensure that the tracking error remains within the RCI tube. Since the RCI tube geometry and control bandwidth is optimized by leveraging the states-dependent uncertainties in the dynamic tube MPC schemes, the proposed robust powered descent guidance can efficiently handle the uncertainties in response to the current conditions with less conservativeness. In Figure 6, thrust magnitude result is described for the maximum disturbance case. The thrust magnitude does not exceed its upper and lower bound even in the presence of unmodeled dynamics and disturbances, which verfies that the thrust magnitude is well tightened by (28).

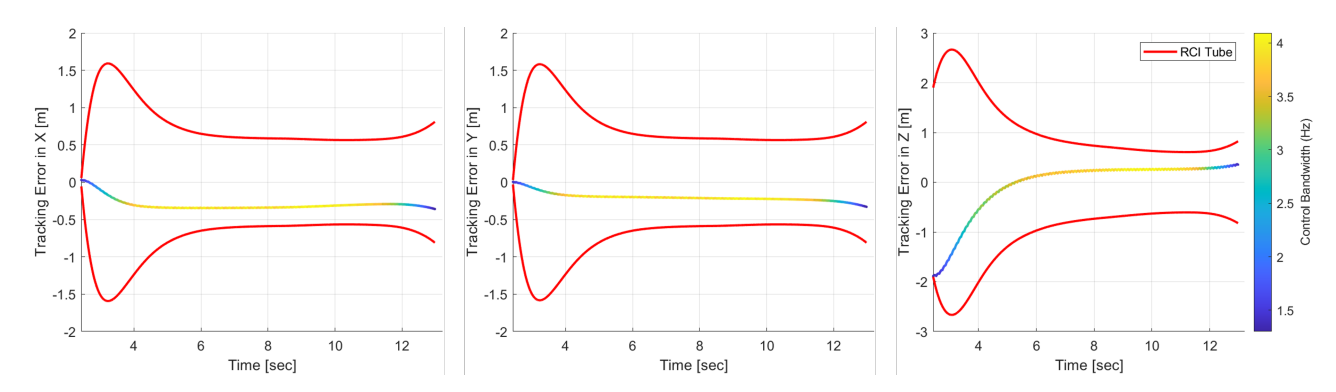


Figure 5 – Tracking error (Maximum Disturbance Case)

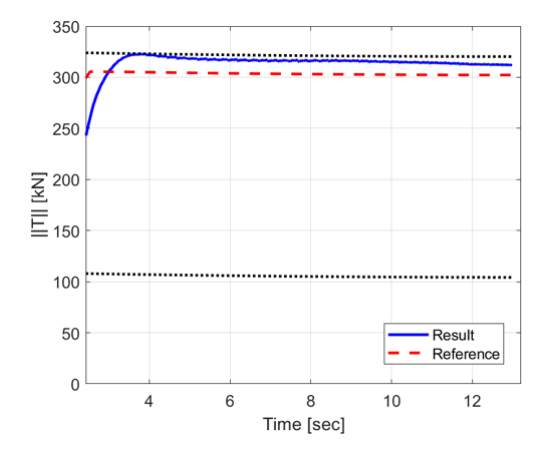


Figure 6 – Thrust magnitude (Maximum Disturbance Case)

5.3 Dispersed Case

To verify the robustness of the proposed PDG algorithm, the Monte Carlo simulation for the dispersed case is conducted with 500 samples. The dispersion values are sampled based on the the distribution described in Table 2 for each simulation. Each value is used as a constant for one simulation, and a newly sampled dispersion value is used for the next Monte Carlo sample.

Figure 7 shows the results of position and velocity trajectory and Figure 8 shows the statistics of the final landing position and velocity of Monte-Carlo samples. The horizontal landing position error has an average of 0.02m with a standard deviation of about 0.2m, indicating that most samples result in precise landing at the desired location. Regarding the final landing speed, horizontal component averages 0.05m/s with a standard deviation of 0.1 m/s and vertical component averages 1.17m/s with 1.3 m/s standard deviation. These results validate the proposed guidance algorithm operates robustly even in the presence of disturbances and modeling errors.

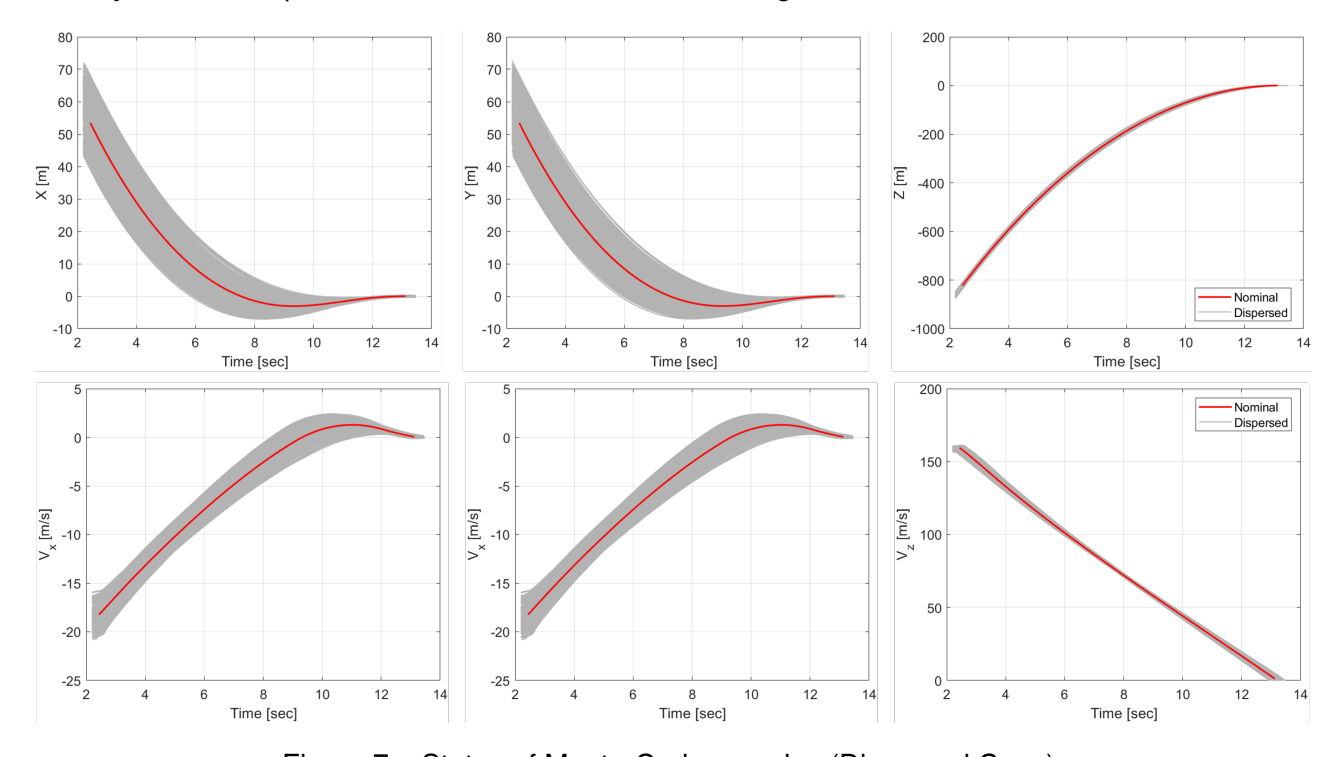


Figure 7 – States of Monte-Carlo samples (Dispersed Case)

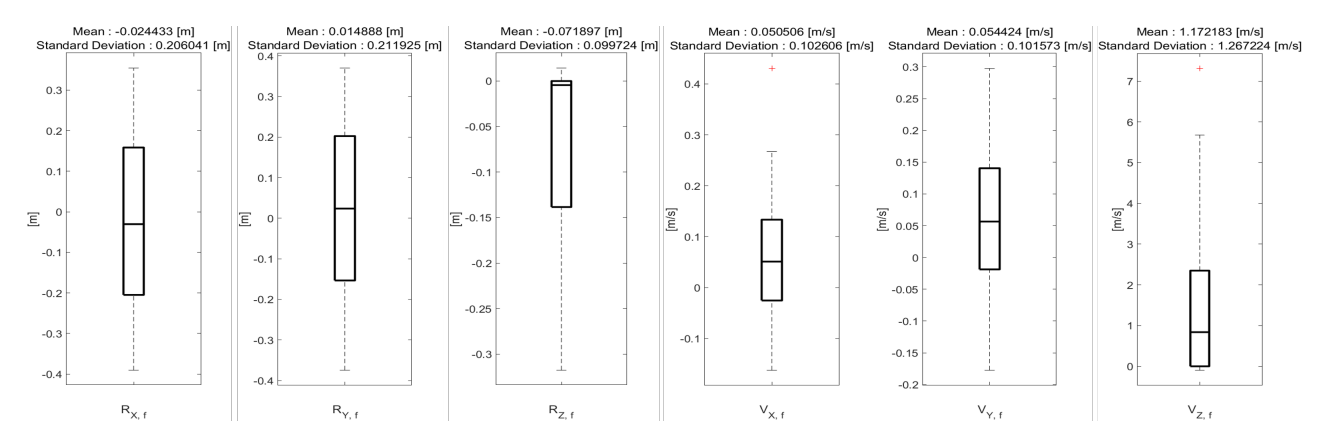


Figure 8 - Final States Statistics (Dispersed Case)

6. Conclusion

This paper presents the robust powered descent guidance formulation through dynamic tube MPC. The MPC problem is formulated based on the powered descent guidance problem for trajectory tracking. The sliding mode controller with boundary layer is utilized as an ancillary controller allowing

to explicitly incorporate the modeling error and external disturbances in the problem. Moreover, robust control invariant tube is derived from the boundary layer of the sliding controller and its tube geometry is simultaneously optimized along with the original states of the PDG problem. The constraints are tightened by taking state-dependent disturbances into account to prevent the constraints violation. The robust PDG problem is finally formulated as a convex optimization framework through lossless convexification and sequential convex programming. The numerical experiments are conducted to validate the performance and robustness of the propsed algorithm and it shows the precise soft landing results even in the presence of modeling error in aerodynamics and external disturbances.

7. Acknowledgement

This work was supported by Institute of Information & communications Technology Planning & Evaluation(IITP) grant funded by the Korea government(MSIT) (No. RS-2023-00223022, Multi-Functional Software for Launch Vehicle Mission Analysis and Design)

8. Contact Author Email Address

Jaell Jang: jji249@kaist.ac.kr

Chang-Hun Lee: lckdgns@kaist.ac.kr Shaoming He: shaoming.he@bit.edu.cn

9. Copyright Statement

The authors confirm that they, and/or their company or organization, hold copyright on all of the original material included in this paper. The authors also confirm that they have obtained permission, from the copyright holder of any third party material included in this paper, to publish it as part of their paper. The authors confirm that they give permission, or have obtained permission from the copyright holder of this paper, for the publication and distribution of this paper as part of the ICAS proceedings or as individual off-prints from the proceedings.

References

- [1] L. Blackmore, "Autonomous precision landing of space rockets," in Frontiers of Engineering: Reports on Leading-Edge Engineering from the 2016 Symposium, The Bridge Washington, DC, 2016, pp. 15–20.
- [2] P. Lu, Ed., "Introducing Computational Guidance and Control," *Journal of Guidance, Control and Dynamics*, vol. 40, no. 2, pp. 193–193, Feb. 2017.
- [3] B. Acikmese and S. R. Ploen, "Convex Programming Approach to Powered Descent Guidance for Mars Landing," *Journal of Guidance, Control and Dynamics*, vol. 30, no. 5, pp. 1353–1366, Sep. 2007.
- [4] X. Liu, "Fuel-Optimal Rocket Landing with Aerodynamic Controls," *Journal of Guidance, Control and Dynamics*, vol. 42, no. 1, pp. 65–77, Jan. 2019.
- [5] M. Szmuk, T. P. Reynolds, and B. Açıkmeşe, "Successive Convexification for Real-Time Six-Degree-of-Freedom Powered Descent Guidance with State-Triggered Constraints," *Journal of Guidance, Control and Dynamics*, vol. 43, no. 8, pp. 1399–1413, Aug. 2020.
- [6] M. Sagliano, "Pseudospectral Convex Optimization for Powered Descent and Landing," *Journal of Guidance, Control and Dynamics*, vol. 41, no. 2, pp. 320–334, Feb. 2018.
- [7] S. P. Boyd and L. Vandenberghe, "Convex optimization," Cambridge, UK; New York: Cambridge University Press, 2004.
- [8] B. T. Lopez, J.-J. E. Slotine, and J. P. How, "Dynamic Tube MPC for Nonlinear Systems," *in 2019 American Control Conference (ACC)*, Philadelphia, PA, USA: IEEE, Jul. 2019, pp. 1655–1662.
- [9] K.W. Jung, S.D. Lee, C.G. Jung, and C.H. Lee, "Model Predictive Guidance for Fuel-Optimal Landing of Reusable Launch Vehicles," *arXiv preprint* arXiv:2405.01264 (2024).
- [10] Y. Mao, M. Szmuk, and B. Acikmese, "Successive convexification of non-convex optimal control problems and its convergence properties," in 2016 IEEE 55th Conference on Decision and Control (CDC), Las Vegas, NV, USA: IEEE, Dec. 2016, pp. 3636–3641.
- [11] J.-J. E. Slotine and W. Li, "Applied nonlinear control," Englewood Cliffs, N.J: Prentice Hall, 1991.
- [12] A. Domahidi, E. Chu, and S. Boyd, "ECOS: An SOCP solver for embedded systems," in 2013 European Control Conference (ECC), Zurich: IEEE, Jul. 2013, pp. 3071–3076.